Quenching Auto-Fluorescence in PMMA-based Devices in Imaging

Pushparani Micheal Raj[1] Elisabetta Stranieri[2] Simona Zaccone[3] Patrizio Candeloro[4] Maria Costanza[5]

[1,2,3,4]BIONEM Laboratory [5]Laboratory of Immunology of Tumors and Immunopathology
[1,2,3,4]Department of Experimental and Clinical Medicine
[1,2,3,4,5]University "Magna Græcia" of Catanzaro, Italy

Abstract— Imaging is a vital part of biological applications, as many profound information could be derived from imaging during various timescales and with labelling, it becomes more crucial. Many POC systems are based on thermoplasts materials and therefore, auto-fluorescence becomes inevitable due to the material nature. In this work, I have presented a simple and yet a smart way to reduce the auto-fluorescence effects on PMMA-like thermoplast material. The work is validated with different types of labelled tumor cells using a inverted fluorescence microscope.

Keywords: PMMA, Autofluorescence, Fluorescence imaging, Optical Window

I. INTRODUCTION

Fluorescence is the emission of light by a material that absorbed light or other forms of electromagnetic radiation, is also known as a form of luminescence. Moreover, the emitted light has a longer wavelength, and therefore lower energy, than the absorbed radiation. The material, therefore, not only simply reflects the absorbed light but also returns a longer wavelength, hence it appears brighter than the original light source [1]. In Fluorescence, this ability to emanate light halts shortly upon removal of the original light source. The time interval from fluorescence excitation to emission is about 10e-9s, which makes fluorescence a good indicator for real-time observations, well explained in Jablonski diagram, of the formation of excited state by absorption and subsequent emission of fluorescence molecules [2]. The fluorescence process is governed by three important phases: excitation, duration and emission. This phenomenon has significantly increased the omnipresent usage of fluorescence in studies and analyses in biology, geography, marine, materials, astronomy and more. Fluorescence has an advantage of providing a very high Signal-to-Noise Ratio (SNR), which allows us to distinguish spatial distributions even of low-concentration species. To use fluorescence, endogenous fluorescence (auto-fluorescence) can be used or the sample can be labeled with a suitable molecule whose distribution will become evident after illumination. The fluorescence microscope is ideal for detecting particular fluorochromes in cells and tissues. The fluorescence microscope, the most common technique, follows the basic design of "fluorescence excitation" which uses filters and a dichroic beam splitter. The object is illuminated with fluorescence excitation light through the same objective lens that collects the fluorescence signal for the image. A ray separator, which transmits or reflects light according to its wavelength, is used to isolate the excitation light from fluorescence light [3, 4].

Auto fluorescence (AF), a natural emission of light by biological structures, also occurs in non-biological materials like porous membranes made of glass fiber, paper like the currency of United States of America and plastics [5-8]. The material of interest discussed in this study is PMMA, which has micro-structures like microfluidic channels of dimensions in the range of few micrometers, created on the surface of PMMA, for various biochemical analyses. The pattern of irregularity like scratch or micro-channels, provoked either during mass production or micro-machining is a problem because the AF from etched or wavy or uneven surfaces is quite significant and not negligible [9-13]. Several studies are organized to reduce or optimize the AF effects in PMMA. Microfluidic chips made of PMMA are assessed under continuous laser illumination and observed that the material undergoes considerable bleaching of AF and resulted in a better visualization [14]. In a wide-range, AF is perceived as a trivial signal over a wide spectrum and when long-pass filter is used, cumulative signal is collected over an extensive range of spectrum and the detector analyzes intensified signal. Perhaps, high-definition detector emerges to be a crucial requisite here which is rather expensive [15, 16]. Alternately, usage of fluorometer as a blank to subtract from the emission or fluorescence microscopy technique (especially confocal) where a line scan gives the signal intensities as a histogram to provide data solely from fluorophore with a negligible amount of emission from the polymer matrix itself are adopted [14]. Glass microfluidic devices for biochemical applications are not offered by PMMA devices, as the former provide exceptional chemical resistance, biocompatibility and optical properties, as well as mechanical stability, which prevents swelling, deformation and AF. Thus, for commercial POC devices, glass becomes a single choice for any fluorescence-based detection, to avoid any worse effects from AF [17].

With the advent of different fluorochromes/fluorophores, specifically targeting different parts of cells or probing diverse ion processes, fluorescence microscopy has shaped a revolution in biology studies and biomaterial classifications. In addition, development of confocal microscopy has greatly expanded the scope of fluorescence microscopy, as it can significantly reduce SNR and further provide quality spectra [4, 18-20]. Nevertheless, reduction of AF in biocompatible plastics like PMMA that is used heavily in LOC and POC devices will embark a massive impact on the usage further. In this work, is presented a passive microfluidic device for chemotaxis studies made of PMMA of total thickness 9 mm. The device exhibited high AF due to the fabricating material that effected on the imaging of fluorescently labeled cells. Hence, an Optical Window (OW) was created on the rear side of the assembled device with a predetermined depth and diameter that enhanced the fluorescence imaging by reducing the AF from the material PMMA.

In the present work, investigations on PMMA microfluidic devices are conducted on the fluorescent markers, Fluorescein is othiocyanate (FITC) and

allophycocyanin (APC) for antibodies and DAPI for nuclei. The antibody labeling used was directed towards the class I major histocompatibility complex (MHC) molecules, and the antibody was then alternatively conjugated to FITC or APC. An important consideration in reporting the fluorophores made with the microscope utilized in the experiments, which allows fluorescence visualization only in DAPI, FITC and Tetramethylrhodamine (TRITC). Henceforth there is a limitation with the use of APC, which was one of the labeling of antibodies. Due to difference in excitation and emission spectra of TRITC and APC [18, 19], poor resolution of TRITC images is reported. Moreover, AF effect is dominant in PMMA and other plastic materials post-thermal treatment, which is the fabrication protocol of the device [14, 21].

II. Optical Window

A. Design & Fabrication

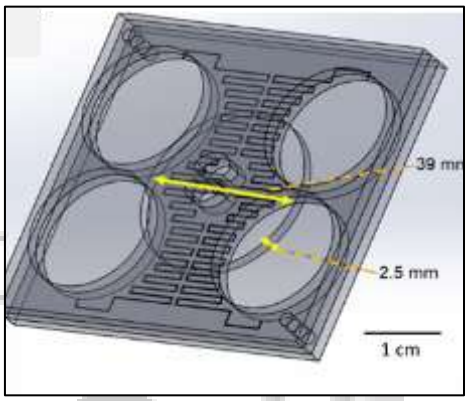

Fig. 1: CAD image of the microfluidic device. Three layers of PMMA and OW at the rear side of the device; Virtually assembled device with OW of 39 mm Ø and 2.5mm depth to enhance imaging resolution

The microfluidic device for chemotaxis studies is made of 3 layers of PMMA and a total thickness of 9 mm. The top layer has 4 side tanks and 2 central tanks, whereas, the middle layer has microchannels that connects the tanks. The bottom layer has only alignment holes and hence is of 3 mm thickness with no additional structures. It is detected during experiments, that, the fluorescently labelled cells had a poor visibility and high SNR under fluorescence microscope due to the auto luminescence property of micro-machined and thermally bonded PMMA layers of the device. Hence, an OW is created at the rear side of bottom layer after the device assembly, as shown in Figure 1. The hollow OW is of 39 mm Ø and 2.5 mm depth, the values are preferred after a series of measurements done in relation to the inverted microscope. The diameter is justified for the largest (in diameter) objective 10× to enable its unrestricted entry/exit through the window for high resolution. Whereas, the depth is determined with working distance of high-resolution lens, 60× objective piece of the microscope. Thereby, both the circumference and working distance of the objectives are optimized with the dimensions of OW. The window readily reduces objective-intermediate layer distance, allowing optimal visualization of cellular migration in fluorescence as in Table 1.

Objective	Lens diameter (mm)	Objective diameter (mm)	Work distance (mm)
10x	18	29.9	15.2
20x	16.1	29.6	8.2 – 6.8
40x	10.1	29.3	3.6 – 2.8
60x	9.2	23.5	2.6 -1.8

Table 1: Characteristics of Microscope

Dimensional characteristics of the objectives of Nikon Eclipse Ti inverted microscope. Based on the values of microscope objective diameter and Work Distance, the OW dimensions are determined

III. OW Fabrication

The assembled device as shown in Figure 1b was repositioned on the work surface of the micro-milling for the creation of OW. The OW is positioned at the center of rear side of device where the central tanks for cells are located and has a Ø of 39 mm and a depth of 2.5 mm. For the construction of this structure, an appropriate design in Solidworks®, which presents the real dimensions of the device, is created. During the initial phase of window fabrication, it is observed that the roughness created by regular milling protocol is high. Hence, to reduce the roughness caused by milling, a pitch of $z \approx 0.1$ mm is handled. This considerably resulted in creating lesser irregularity and the final device with OW is displayed in Figure 2.

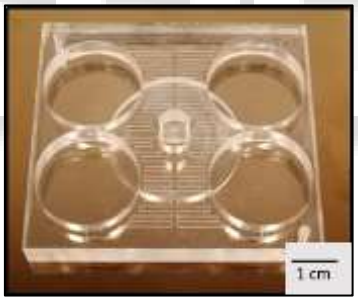

Fig. 2: Final Device with OW. The assembled device is repositioned on the micro-cutter and window is machined with reduced z-pitch for lesser roughness on the rear side

A. Optimization

1) Roughness in OW

Following the accomplishment of OW using micro-milling technique, it was mandatory to promote the conditions for fluorescence analyzes. The pocketing technique (micro-milling) used, emanated substantial fallacious changes on the surface of the device that inflicts poor visibility of cells (Figure 3). It was noticed that concentric circles with irregular roughness, on the surface created by the micro tool, during manufacturing, making it unappealing for visualization. This roughness posed to be a paramount limitation for fluorescence visualizations, which are already difficult in PMMA. For this reason, it was necessary to carry out studies to diminish this roughness, to obtain a surface that is as smooth and translucent as possible with the OW. For these studies, a workpiece of PMMA of 3 mm thickness, with 9 OWs of 29 mm Ø and 0.5 mm depth is constructed using

micro-milling, leaving the real device parameters unchanged. Each test window was utilized for a unique protocol and in conclusion the best condition for glass finish was adopted for the definite studies.

Fig. 3: Detail of the OW under optical microscope. It is visible for the concentric structures created because of milling. Hence, reduction of roughness is obligatory for better visualization

2) Methods for roughness reduction

PMMA (commonly known as Plexiglas®), has among its features a strong scratch and abrasion resistance, which is why it is easily repairable if some external factors like temperature, pressure break through the resistance and stain the material [22-24]. High transparency makes PMMA an ideal replacement for glass where cost, handling, weight or temperature is a grave issue. Nevertheless, a scratch despite having a little influence on the durability, over time, may emerge as flaw to break the system because, optical and mechanical properties are directly influenced by the microstructure of PMMA [25]. In this study, when the prime concern was to obtain a polished surface without any roughness on the OW, trivial scratches were additional. To restore such minor yet critical damages, optical grade sandpaper and abrasive paste is profiting. The choice of optical grade is in relation to PMMA, which is optically transparent, and similarly, choice of grit size is proportional to the roughness present on the surface to be worked. As it is well known, grit size refers to the size of the particles of abrading materials embedded in the sandpaper.

Several standards are already established, that, not only provide the average grit size, but also the allowable variation from the average, such as United States CAMI (Coated Abrasive Manufacturers Institute) and the European FEPA (Federation of European Producers of Abrasives). The FEPA system is the same as the ISO 6344 standard. Thus, to start with, the roughness in the device is measured by profilometer with the analysis on Roughness Average (Ra) parameter.

The best fit to determine the type of sandpaper that suits the objective, is to learn about abrasive materials and their properties. For plastic materials there are two types of optimal sandpaper: aluminum oxide and silicon carbide. In this work, silicon carbide sandpaper was used, as it removes materials quicker than aluminum oxide. Regardless, for the grit size it represents the size of abrasive particles. The lower the number, the larger the abrasive particles, which means they remove more material still create noticeable scratches. A higher number, on the other hand, indicates smaller particles that hardly removes any material, though leave a finer and more polished appearance. The sanding projects use different grain sizes in general, starting from grains with lower numbers and moving the scale towards finer and higher grits. Each higher grain removes scratches from the previous grain, creating an increasingly smooth surface [26].

Window #	Roughness Average (µm)	
	Internal	External
Window 1	0.3737±0.2253	1.9224±1.9224
Window 2	0.2061±0.033	0.4129±0.1055
Window 3	0.2171±0.038	0.3850±0.1064
Window 4	0.2622±0.076	0.4738±0.0890
Window 5	0.3048±0.0511	0.4112±0.1381
Window 6	0.2685±0.0794	0.4533±0.0998
Window 7	0.2042±0.1096	0.3741±0.1525
Window 8	0.2399±0.0329	0.5126±0.3331
Window 9	0.2132±0.0539	0.3468±0.0875

Table 2: Ra of the 9 OWs calculated

This window was utilized to test different methods of roughness reduction until the optimal protocol was finalized

Protocol	Roughness [Å]	
	Internal	External
Initial	2705.4	529.1
After Soap-based Abrasion	2333.7	414.2
After Solvent-Based Abrasion	1517.4	398.6
Initial	4032.3	432
After Solvent-Based Abrasion	2684.4	326.7
After Soap-based Abrasion	3030.6	224.8

Table 3: Results of Abrasion

The data obtained from abrasive pastes, soap-based and solvent-based, clearly shows that the abrasion effect of soap-based paste is lesser when compared to solvent-based

In this work, a single optical grade sandpaper (Dremel Kit – Extra fine 240-Grit) with a grain size of 50 microns was used based on the profilometer calculations for two surface roughness levels present on the test piece with 9 windows and results are listed in Table 2. A high roughness was observed between the grooves and a lower roughness between contours. Similarly, for removal of finer scratches and produce a satin finish after sanding, two abrasive pastes were employed, 726 grade – Superpast from Corcos®, a solvent-based polishing paste and Chromglanz from Kerstens Original®, a soap-based polishing paste [27]. It is thoroughly understood that these pastes are conducive to be used with PMMA. With the initial tests using the pastes, it is observed that, solvent-based paste was more aggressive on the reduction of roughness when compared to soap-based as mentioned in Table 3. Therefore, the decision to use the soap-based followed by solvent-based to achieve more polished and optically transparent structure is adopted.

Moreover, there was another physical parameter in influence while sanding and polishing – Temperature. The effect of temperature upon sanding due to the friction between sandpaper and removed material, was inevitable, resulting in a slightly elevated temperature. The fabric in place for application of pastes is Microfiber, a synthetic fiber finer than one denier, having a diameter of less than ten micrometers. Therefore, it was concluded to use a wet fabric, immersed in distilled water, to apply with abrasive pastes [28-30]. There was a significant impact on roughness reduction with the use of dampened fabric.

The protocol to remove roughness is as follows.

1) Hard and rough sanding of OW with sandpaper (P240)
2) Application of soap-based abrasive paste for a total of 30 revolutions
3) Application of solvent-based abrasive paste for a total of about 700 revolutions

IV. RESULTS

The results obtained are displayed in Figure 5, showing the multiple steps performed until the final satin finish is obtained. It is also apparent that the reduction of roughness was evident through the 9-window test, shown in Figure 6. A graph to illustrate the reduction trend is drawn (Figure 7). All fluorescent images were taken at room temperature using a Nikon Eclipse Ti inverted fluorescent microscope with PlanFluor 10×, 20×, 40× and 60× objectives coupled to a Nikon DS-Qi1Mc CCD camera (Nikon Instruments). Three filters for three different excitation/emission wavelengths were available, DAPI, FITC and TRITC. Images were acquired with NIS-Elements Version D software (Nikon Instruments). Image analysis for fluorescence tests on labeled samples were performed in ImageJ with custom macros and plugins.

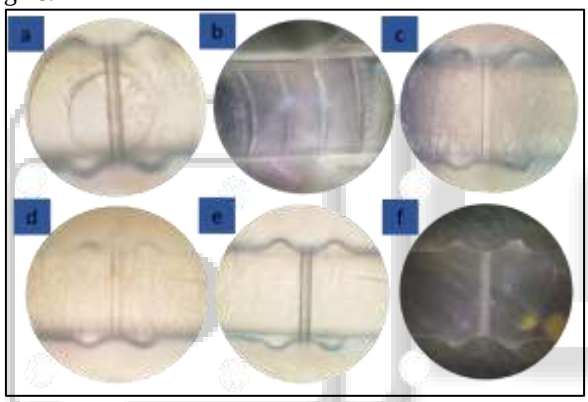

Fig. 4: Demonstration of the reduction of roughness a-f. a) Image of the initial roughness in BF mode, note the contours below the transverse channel; b) Image in dark-field mode; c) Following the sanding process roughness of contours are removed, however the device has gained a lot of scratches; d) Scratches are reduced following the application of soap-based abrasive paste, e) Image of the final optimized roughness in BF mode; f) Image of final roughness optimized in dark-field

To validate the ultimate functioning of OW, diverse experiments were performed with fluorescently labeled cells. The cells used for these experiments are Jurkat cells of suspension line, i.e., acute T-cell leukemia lymphoblasts. The medium and cells were kindly granted by the Laboratory of Immunology of Tumors and Immunopathology (L.I.T.I.P) of University "Magna Græcia of Catanzaro, Italy". To elucidate the work, images collected using devices presented with different conditions and objectives at different resolutions were compared.

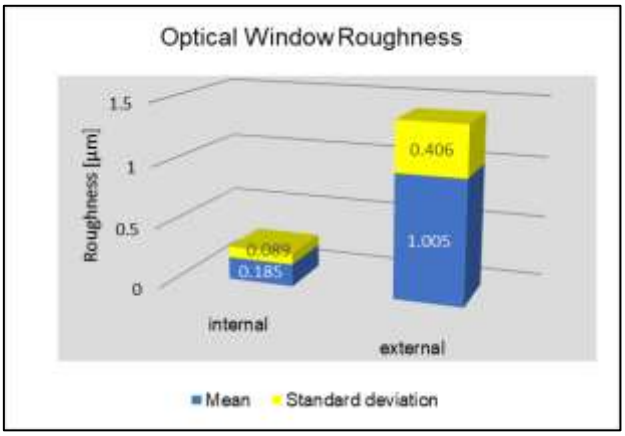

Fig. 5: Graph of the roughness values of OW. Account the considerable difference between the internal and external values of the groove. In accordance with the images in fig 4, application of sandpaper resulted in an increased roughness and yet almost removed the concentric circles. The minimum value obtained is approximately equal to 0.14 µm

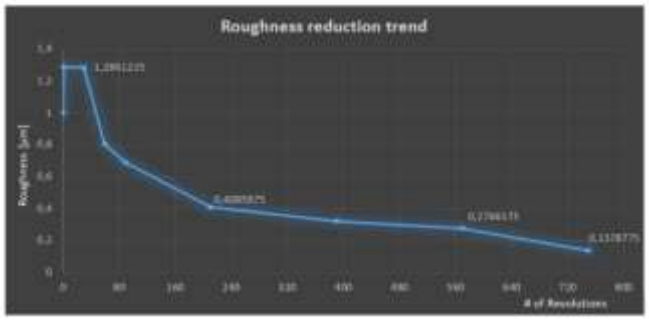

Figure 6: The trend of reduction of roughness. The values of external roughness before and after optimization is displayed

Imaging and Analysis were performed with the following devices:

1) Microfluidic device without OW (WOW)
2) Microfluidic device unworked rough OW (OWR)
3) Microfluidic device with reduced roughness (OWRR)
4) Microfluidic device with reduced roughness in contact with glass on the surface of lens oil (OWRRO)

Oil immersion is a technique in light microscopy, to increase the resolving power of a microscope by immersing both the objective lens and the specimen in a transparent oil of high refractive index, thereby increasing the numerical aperture of the objective lens [31]. A little drop (< 1µl) of Nikon Immersion Oil for Microscopy Type A of refractive index 1.515 is used in this study between the layer of OW and glass slide. The images in Figure 7 to 10 displays micrographs in bright-field (BF) and for the three different fluorophores (DAPI, FITC and TRITC).

Through the images shown in Figure 7, it is possible to distinguish the visualization effects of BF images of the labeled cells. However, it was determined that the cells were optimally viewed under OWRR and OWRRO. In Figure 8, FITC images are displayed for 10× as cells were not visible due to the labeling technique on the antibodies. Figure 9 illustrates that the best results were procured in DAPI, as it is possible to exhibit the core marking with the objectives from 10x to 60x, although obviously with the 40x and 60x objectives the definition of the cell is not as precise as with

the other magnifictaion. For TRITC, instead, good results were achieved through 20x objectives (Figure 10).

A. Bright-Field Images

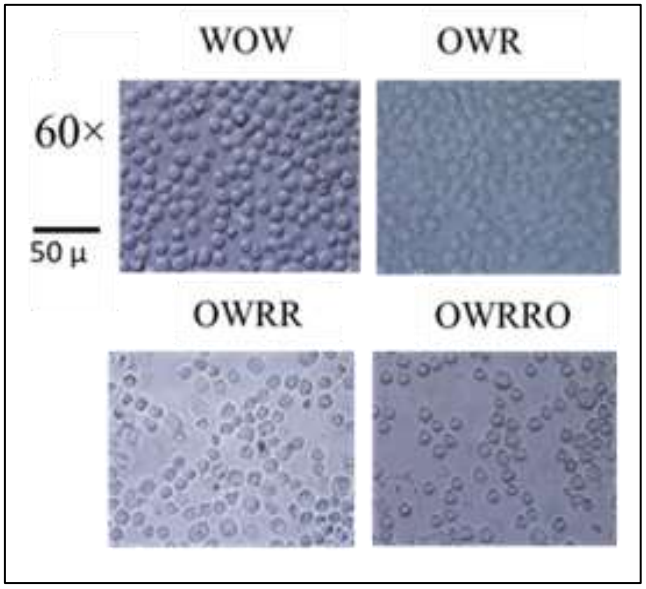

Fig. 7: Visualization of cells in BF. BF images of labeled cells in 60×, optimal results were obtained from WOW, OWRR and OWRRO

B. FITC Images

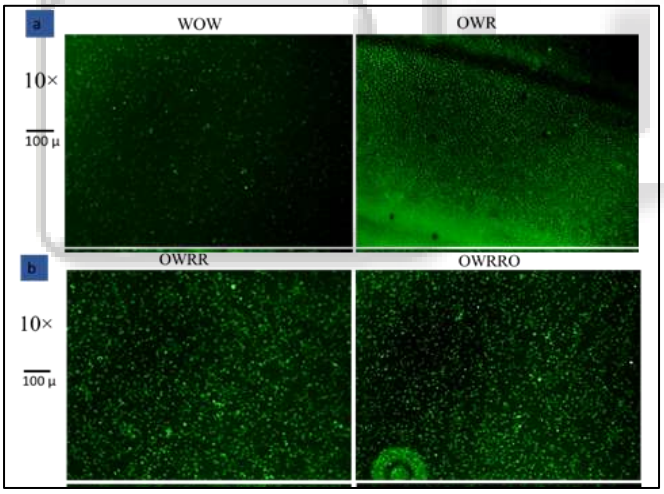

Figure 8: Visualization of cells in FITC a-b. Images of FITC labeled cells in 10× because the cells were labeled in antibodies. a) 10× bare visibility of cell population in WOW, whereas in OWR, the device exhibited AF which was not appreciated; b) In OWRR and OWRRO the cells with highly reduced AF enhanced to view cell density. Nevertheless, cells were in near precision under OWRR and the best results were with OWRRO

C. DAPI Images

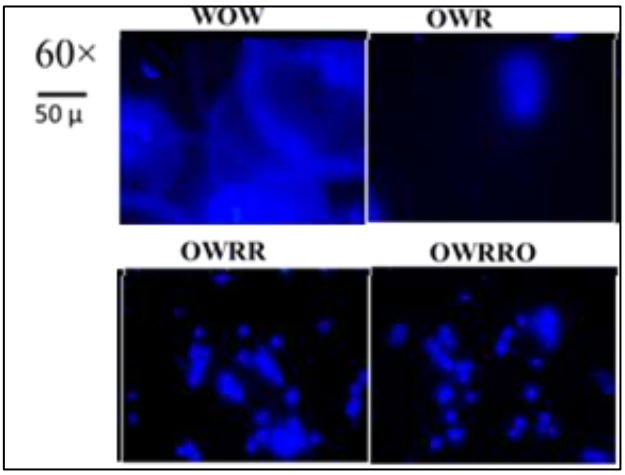

Fig. 9: Visualization of cells in DAPI. Images of DAPI labeled cells in 60× as the cells were labeled in nuclei. WOW did not have good resolution of cells. OWR always had AF issue whereas OWRR and OWRRO had best results

D. TRITC Images

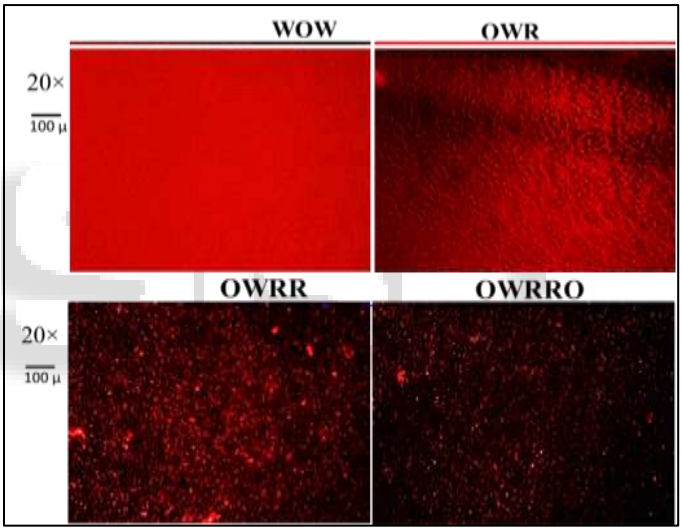

Fig. 10: Visualization of cells in TRITC. Images of APC labeled cells under TRITC mode of microscope, in 20× because the cells were labeled in antibodies. In WOW the cells were faintly visible with intense AF and, OWR with high background signal meager cell visibility; whereas in OWRR and OWRRO the cells were visible with increased density than WOW.

It can be stated with certainty that there is a noticeable improvement in the fluorescence visualization through the implementation of the OW, by reducing the thickness of PMMA. In addition, the optimization protocol for the sanding of PMMA layer in OW and subsequent usage of abrasive pastes with wetted fabric enhanced the visualization effects on the labeled cells.

V. CONCLUSION

The work has established microfluidic platforms to deploy innumerable characteristics of the microenvironment of cells in culture and chemotaxis. An innovative feature, OW, implemented in this present work for clear visualization of fluorescently labeled cells. By virtue of easy operation and

passive pumping method, a contamination-free environment is promised with these devices. In addition, the high optical quality PMMA is suitable for live-cell investigations and fluorescence studies.

The device allowed visualization of fluorescently labeled cells, despite the limitations deriving from the use of PMMA. Like other thermoplastic materials, PMMA is most desirable in biochemical analyses for the low-cost and flexible manufacturing properties. The behavior of the presented device is highly satisfactory: verifying that the implementation of cellular fluorescence is feasible in microfluidic systems that constitutes the fundamental step and significant result in relation to the purpose and objectives initially proposed.

ACKNOWLEDGMENTS

The author gratefully acknowledges the Italian Ministry of Health for the support grant for the current research activity

REFERENCES

[1] R. W. Wood, "The time interval between absorption and emission of light in fluorescence," *Royal Society of Chemistry*, vol. 99, no. 100, 1921.
[2] S.-W. Lin, C.-H. Chang, and C.-h. Lin, "High-throughput Fluorescence Detections in Microfluidic Systems," *Genomic Med Biomark Health Sci*, vol. 3(1), pp. 27-38, 2011.
[3] P. Campagnola *et al.*, "Biophotonics feature: introduction," *Biomed Opt Express*, vol. 9, no. 3, pp. 1229-1231, Mar 1 2018, doi: 10.1364/BOE.9.001229.
[4] P. N. Prasad, "Introduction to biophotonics," *John Wiley & Sons*, 2003.
[5] G. E, M. S, and U. KO, "Advances in microfluidic devices made from thermoplastics used in cell biology and analyses," *Biomicrofluidics*, vol. 11(5), 2017.
[6] K. G. Shah and P. Yager, "Wavelengths and Lifetimes of Paper Autofluorescence: A Simple Substrate Screening Process to Enhance the Sensitivity of Fluorescence-Based Assays in Paper," *Anal Chem*, vol. 89, no. 22, pp. 12023-12029, Nov 21 2017, doi: 10.1021/acs.analchem.7b02424.
[7] T. H. Chia and M. J. Levene, "Detection of counterfeit U.S. paper money using intrinsic fluorescence lifetime," *Opt Express*, vol. 17, no. 24, pp. 22054-61, Nov 23 2009, doi: 10.1364/OE.17.022054.
[8] A. Piruska *et al.*, "The autofluorescence of plastic materials and chips measured under laser irradiation," *Lab Chip*, vol. 5, no. 12, pp. 1348-54, Dec 2005, doi: 10.1039/b508288a.
[9] J. Emmelkamp *et al.*, "The potential of autofluorescence for the detection of single living cells for label-free cell sorting in microfluidic systems," (in eng), *Electrophoresis*, Research Support, Non-U.S. Gov't vol. 25, no. 21-22, pp. 3740-5, Nov 2004, doi: 10.1002/elps.200406070.
[10] M. F. Devaux *et al.*, "Synchrotron Time-Lapse Imaging of Lignocellulosic Biomass Hydrolysis: Tracking Enzyme Localization by Protein Autofluorescence and Biochemical Modification of Cell Walls by Microfluidic Infrared Microspectroscopy," (in eng), *Front Plant Sci*, vol. 9, p. 200, 2018, doi: 10.3389/fpls.2018.00200.
[11] N. Bao, B. Jagadeesan, A. K. Bhunia, Y. Yao, and C. Lu, "Quantification of bacterial cells based on autofluorescence on a microfluidic platform," (in eng), *J Chromatogr A*, Research Support, U.S. Gov't, Non-P.H.S. vol. 1181, no. 1-2, pp. 153-8, Feb 15 2008, doi: 10.1016/j.chroma.2007.12.048.
[12] E. P. Boets, J. H. Kok, and J. A. van Best, "The blue-green autofluorescence of the human ocular lens after the wear of PMMA contact lenses," (in eng), *Acta Ophthalmol (Copenh)*, vol. 72, no. 1, pp. 67-71, Feb 1994. [Online]. Available: http://www.ncbi.nlm.nih.gov/pubmed/8017200.
[13] H. Miyashita, T. Ooie, T. Nakahara, and Y. Baba, "Autofluorescence of Electrophoresis Chip Grooved by Excimer Laser," *Journal of Laser Micro / Nanoengineering*, vol. 3(2), pp. 88-94, 2008.
[14] A. Piruska *et al.*, "The autofluorescence of plastic materials and chips measured under laser irradiation," (in eng), *Lab Chip*, Research Support, N.I.H., Extramural vol. 5, no. 12, pp. 1348-54, Dec 2005, doi: 10.1039/b508288a.
[15] O. Hofmann *et al.*, "Monolithically integrated dye-doped PDMS long-pass filters for disposable on-chip fluorescence detection," (in eng), *Lab Chip*, Research Support, Non-U.S. Gov't vol. 6, no. 8, pp. 981-7, Aug 2006, doi: 10.1039/b603678c.
[16] S. Diao *et al.*, "Biological imaging without autofluorescence in the second near-infrared region," *Nano Research*, vol. 8, no. 9, pp. 3027-3034, 2015.
[17] M. R. H. Hyungjun Jang 1 ID , Youngkyu Kim, Jun Kim, Pyoung-hwa Oh,Jonghyun Ju, Seok-Min Kim and Jiseok Lim, "Fabrication of Glass Microchannel via Glass Imprinting using a Vitreous Carbon Stamp for Flow Focusing Droplet Generator," *Sensors-Basel*, vol. 18, no. 83, 2017.
[18] R. P. Haugland, "Spectra of fluorescent dyes used in flow cytometry," (in eng), *Methods Cell Biol*, vol. 42 Pt B, pp. 641-63, 1994. [Online]. Available: http://www.ncbi.nlm.nih.gov/pubmed/7533258.
[19] B. Bruijns, R. Tiggelaar, and H. Gardeniers, "Dataset of the absorption, emission and excitation spectra and fluorescence intensity graphs of fluorescent cyanine dyes for the quantification of low amounts of dsDNA," (in eng), *Data Brief*, vol. 10, pp. 132-143, Feb 2017, doi: 10.1016/j.dib.2016.11.090.
[20] C. P. Toseland, "Fluorescent labeling and modification of proteins," (in eng), *J Chem Biol*, Review vol. 6, no. 3, pp. 85-95, Apr 13 2013, doi: 10.1007/s12154-013-0094-5.
[21] E. W. Young, E. Berthier, and D. J. Beebe, "Assessment of enhanced autofluorescence and impact on cell microscopy for microfabricated thermoplastic devices," (in eng), *Anal Chem*, Research Support, Non-U.S. Gov't Research Support, U.S. Gov't, Non-P.H.S. vol. 85, no. 1, pp. 44-9, Jan 2 2013, doi: 10.1021/ac3034773.
[22] Z. Vuluga *et al.*, "Morphological and Tribological Properties of PMMA/Halloysite Nanocomposites," (in eng), *Polymers-Basel*, vol. 10, no. 8, Jul 25 2018, doi: 10.3390/polym10080816.

[23] G. Beadie, M. Brindza, R. A. Flynn, A. Rosenberg, and J. S. Shirk, "Refractive index measurements of poly(methyl methacrylate) (PMMA) from 0.4-1.6 mum," (in eng), *Appl Opt*, vol. 54, no. 31, pp. F139-43, Nov 1 2015, doi: 10.1364/AO.54.00F139.
[24] Z. T. Al-Aqbi, Y. C. Yap, F. Li, and M. C. Breadmore, "Integrated Microfluidic Devices Fabricated in Poly (Methyl Methacrylate) (PMMA) for On-site Therapeutic Drug Monitoring of Aminoglycosides in Whole Blood," (in eng), *Biosensors (Basel)*, vol. 9, no. 1, Jan 30 2019, doi: 10.3390/bios9010019.
[25] E. A. Campo, "The Complete Part Design Handbook: For Injection Molding of Thermoplastics," *Hanser*, 2006.
[26] M. P. Schultz, "The Relationship Between Frictional Resistance and Roughness for Surfaces Smoothed by Sanding," *J. Fluids Eng*, vol. 124, pp. 492-499, 2002.
[27] H. f. Plexiglass, "Surface Treatment of PLEXIGLAS® Guidelines for Workshop Practice," 2008.
[28] M. C. d. S. Alves, L. F. F. Santiago, M. T. T. Gonçalves, I. D. D. Valarelli, and F. M. F. d. A. Varasquim, "EFFECTS OF BELT SPEED, PRESSURE AND GRIT SIZE ON THE SANDING OF Pinus elliottii WOOD," *CERNE*, vol. 21, no. 1, 2015.
[29] W. Tang, B. Bhushan, and S. Ge, "Friction, adhesion and durability and influence of humidity on adhesion and surface charging of skin and various skin creams using atomic force microscopy," *J Microsc*, vol. 239, no. 2, pp. 99-116, Aug 1 2010, doi: 10.1111/j.1365-2818.2009.03362.x.
[30] A. Arcifa, A. Rossi, R. M. Espinosa-Marzal, and N. D. Spencer, "Influence of Environmental Humidity on the Wear and Friction of a Silica/Silicon Tribopair Lubricated with a Hydrophilic Ionic Liquid," *ACS Appl Mater Interfaces*, vol. 8, no. 5, pp. 2961-73, Feb 10 2016, doi: 10.1021/acsami.5b09370.
[31] S. F. Gibson and F. Lanni, "Experimental test of an analytical model of aberration in an oil-immersion objective lens used in three-dimensional light microscopy," *Journal of the Optical Society of America A*, vol. 9, no. 1, pp. 154-166, 1992.

